iScience

CellPress
OPEN ACCESS

Article

Modeling SARS-CoV-2 infection and its individual differences with ACE2-expressing human iPS cells

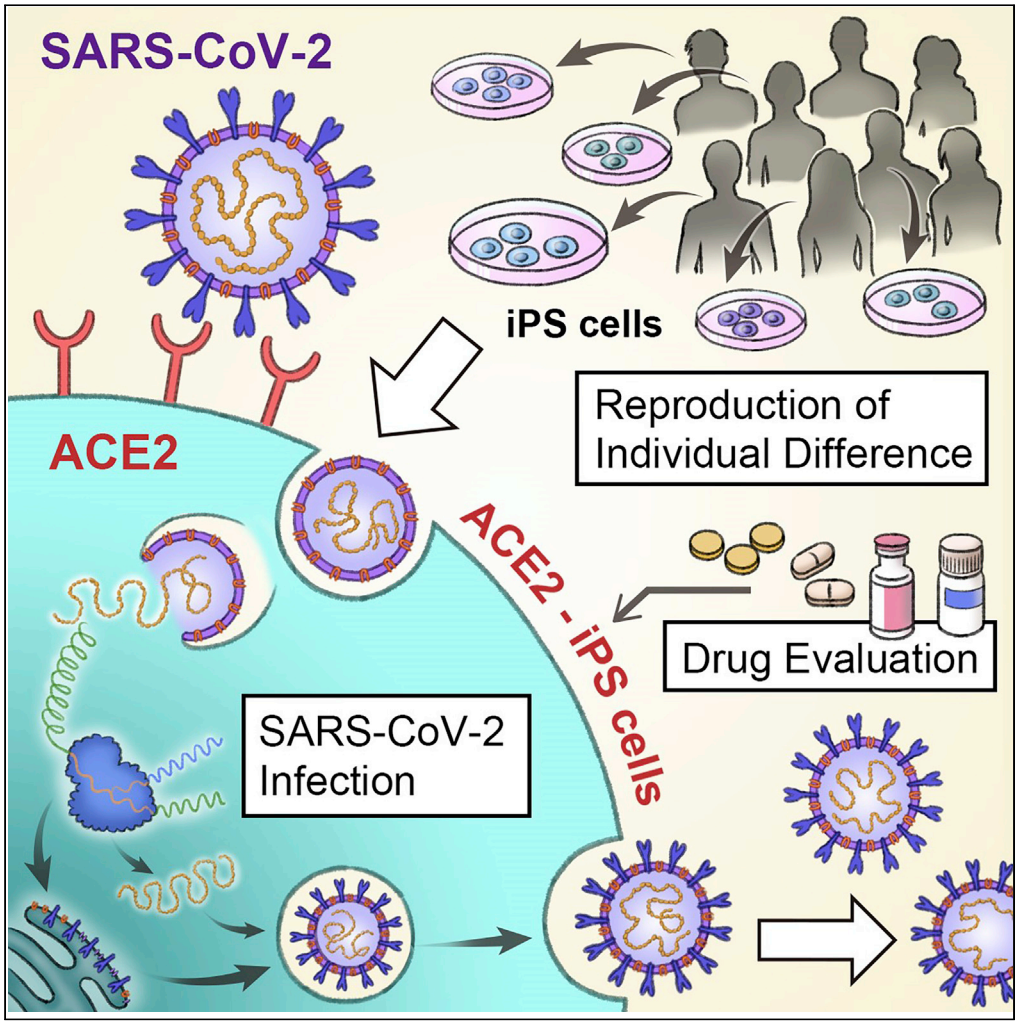

Emi Sano, Sayaka Deguchi, Ayaka Sakamoto, ..., Takeshi Noda, Takuya Yamamoto, Kazuo Takayama

kazuo.takayama@cira.kyoto-u.ac.jp

Highlights

ACE2 expression is required for SARS-CoV-2 to infect human iPS cells

SARS-CoV-2 life cycle can be reproduced in the ACE2-iPS cells

COVID-19 candidate drugs can be evaluated using ACE2-iPS cells

ACE2-iPS cells can reproduce individual differences in SARS-CoV-2 infection

Sano et al., iScience 24, 102428
May 21, 2021
https://doi.org/10.1016/j.isci.2021.102428

iScience

CellPress
OPEN ACCESS

Article

Modeling SARS-CoV-2 infection and its individual differences with ACE2-expressing human iPS cells

Emi Sano,[1] Sayaka Deguchi,[1] Ayaka Sakamoto,[1] Natsumi Mimura,[1] Ai Hirabayashi,[2,3] Yukiko Muramoto,[2,3] Takeshi Noda,[2,3] Takuya Yamamoto,[1,4,5,6] and Kazuo Takayama[1,7,*]

SUMMARY

Genetic differences are a primary reason for differences in the susceptibility and severity of COVID-19. As induced pluripotent stem (iPS) cells maintain the genetic information of the donor, they can be used to model individual differences in SARS-CoV-2 infection *in vitro*. We found that human iPS cells expressing the SARS-CoV-2 receptor angiotensin-converting enzyme 2 (ACE2) (ACE2-iPS cells) can be infected w SARS-CoV-2. In infected ACE2-iPS cells, the expression of SARS-CoV-2 nucleocapsid protein, budding of viral particles, and production of progeny virus, double membrane spherules, and double-membrane vesicles were confirmed. We performed SARS-CoV-2 infection experiments on ACE2-iPS/ embryonic stem (ES) cells from eight individuals. Male iPS/ES cells were more capable of producing the virus compared with female iPS/ES cells. These findings suggest that ACE2-iPS cells can not only reproduce individual differences in SARS-CoV-2 infection *in vitro* but also are a useful resource to clarify the causes of individual differences in COVID-19 due to genetic differences.

INTRODUCTION

The number of patients with coronavirus disease 2019 (COVID-19) and deaths continues to rise. Interestingly, the symptoms of COVID-19 are known to vary widely among individuals and include asymptomatic cases. Genetic differences are one cause for the differences in susceptibility and severity of COVID-19 (Anastassopoulou et al., 2020; Group, 2020; Pairo-Castineira et al., 2021; Zeberg and Pääbo, 2020). Approximately 20% of patients infected with severe acute respiratory syndrome coronavirus 2 (SARS-CoV-2) will present severe symptoms (Weiss and Murdoch, 2020). To develop drugs for patients with severe COVID-19, it is necessary to identify the causes of the worsening symptoms. Although several models, including cells such as Vero, Calu-3, and Caco-2 cells; organoids; and animals such as angiotensin-converting enzyme 2 (ACE2)-transgenic mice, hamsters, and ferrets have been used to study SARS-CoV-2 infection (Takayama, 2020), they do not reproduce individual differences well.

Human induced pluripotent stem (iPS) cells can be established from any individual (Takahashi et al., 2007). Furthermore, they are widely used as genetic disease models because they inherit the genetic information of their donors (Park et al., 2008). Our institute (Center for iPS Cell Research and Application, CiRA) has established iPS cells from more than 500 individuals. As this iPS cell panel was established from a human population of diverse genetic backgrounds, it can be a resource for reproducing individual differences in response to pathogens and drugs. Accordingly, in this study, we attempted to reproduce the SARS-CoV-2 infection and its individual differences using this panel.

It has been reported that SARS-CoV-2 infection is dependent on the expression of ACE2 and transmembrane protease, serine 2 (TMPRSS2) in host cells (Hoffmann et al., 2020). Type II alveolar epithelial cells, bronchial ciliated cells, pharyngeal epithelial cells, and intestinal epithelial cells all express high levels of ACE2 (Ziegler et al., 2020) and can be easily infected by SARS-CoV-2. It has also been reported that embryonic stem (ES) cell-derived type II alveolar epithelial cells and intestinal epithelial cells can be infected with SARS-CoV-2 (Han et al., 2021). However, the investigation of infection differences at the individual level and at large scale using iPS cell-derived somatic cells is hindered by the long time (generally more than 3 weeks)

[1]Center for iPS Cell Research and Application (CiRA), Kyoto University, Shogoin Kawaharacho 53, Sakyo-ku, Kyoto 606-8507, Japan

[2]Laboratory of Ultrastructural Virology, Institute for Frontier Life and Medical Sciences, Kyoto University, Kyoto 606-8507, Japan

[3]CREST, Japan Science and Technology Agency (JST), Kawaguchi 332-0012, Japan

[4]Institute for the Advanced Study of Human Biology (WPI-ASHBi), Kyoto University, Kyoto 606-8501 Japan

[5]Medical-risk Avoidance Based on iPS Cells Team, RIKEN Center for Advanced Intelligence Project (AIP), Kyoto 606-8507, Japan

[6]AMED-CREST, Japan Agency for Medical Research and Development (AMED), Tokyo 100-0004, Japan

[7]Lead contact

*Correspondence: kazuo.takayama@cira.kyoto-u.ac.jp

https://doi.org/10.1016/j.isci.2021.102428

to differentiate the iPS cells and the variable differentiation efficiency among iPS cell lines (Kajiwara et al., 2012). SARS-CoV-2 infection experiments in undifferentiated iPS cells would reduce the time.

However, due to the low expression of ACE2 and TMPRSS2, SARS-CoV-2 does not infect iPS cells. Therefore, in this study, we identified SARS-CoV-2-related genes that enable SARS-CoV-2 to infect undifferentiated human iPS cells. To facilitate gene overexpression experiments with multiple iPS cell lines, we used adenovirus (Ad) vectors. Because the gene transfer efficiency of Ad vectors to undifferentiated iPS cells is almost 100%, there was no need to obtain clones expressing SARS-CoV-2-related genes. Next, we investigated whether the life cycle of SARS-CoV-2 can be reproduced in iPS cells expressing these SARS-CoV-2-related genes. We also show the value of ES/iPS cells to test drugs and gender effects. Our findings indicate that iPS cells expressing SARS-CoV-2-related genes are useful for the study of SARS-CoV-2 infection and its individual patient differences.

RESULTS

SARS-CoV-2 does not infect undifferentiated iPS cells

First, we examined whether undifferentiated iPS cells could be infected by SARS-CoV-2 (Figure S1A). Before conducting this experiment, we examined the expression levels of viral receptors and proteases in undifferentiated iPS cells (Figure S1B). The gene expression level of *ACE2* was low, but that of *CD147* was high. CD147 is reported as a coronavirus receptor (Wang et al., 2020). TMPRSS2, a protease, was also expressed in undifferentiated iPS cells. We thus tried to infect undifferentiated iPS cells with SARS-CoV-2, but the morphology of the iPS cell colonies did not change (Figure S1C). In addition, viral genome in the cell culture supernatant (Figure S1D) and the production of infectious virus (Figure S1E) were not detected. The gene expression levels of undifferentiated markers (Figure S2A) and innate immune response-related markers (Figure S2B) were also unchanged. Furthermore, the expression of SARS-CoV-2 nucleocapsid (N) protein was not detected (Figure S2C). Together, these results indicated that SARS-CoV-2 does not infect undifferentiated iPS cells.

ACE2 expression is required for SARS-CoV-2 to infect human iPS cells

As human ACE2 and TMPRSS2 are known to be important for SARS-CoV-2 to infect cells, we overexpressed human ACE2 and TMPRSS2 in undifferentiated iPS cells by using Ad vectors (Figure 1A). The overexpression of ACE2 in iPS cells (ACE2-iPS cells) caused a large amount of SARS-CoV-2 infection (Figure 1B). Additionally, the amount of viral genome in the cell culture supernatant increased (Figure 1C). This was not the case if only overexpressing TMPRSS2. Furthermore, 2 days after the ACE2-iPS cells were infected with SARS-CoV-2, cell fusion was observed (Figure 1D), and after 4 days many of the cells died. Therefore, these results indicate that ACE2 expression is required for SARS-CoV-2 to infect undifferentiated iPS cells.

Characterization of SARS-CoV-2-infected ACE2-iPS cells

Transmission electron microscopic (TEM) images of ACE2-iPS cells infected with SARS-CoV-2 were obtained (Figures 2 and S3). Zippered endoplasmic reticulum (ER) (Figure 2B), double-membrane spherules (DMS) (Figure 2B) (Maier et al., 2013), and viral particles near the cell membrane (black arrow) (Figure 2D) were observed. So was an ER-Golgi intermediate compartment (ERGIC) containing SARS-CoV-2 particles (black arrows) (Figures 2C and S3). Double-membrane vesicles (DMVs, black arrows) were also observed in infected ACE2-iPS cells (Figure S3). DMVs are the central hubs for viral RNA synthesis (Klein et al., 2020). These structures were not observed in uninfected ACE2-iPS cells. These TEM images show that the life cycle of SARS-CoV-2 can be observed in ACE2-iPS cells.

Next, we analyzed gene and protein expressions in uninfected and infected iPS cells 3 days after the viral infection. The intracellular viral genome and *ACE2* expression levels in ACE2-iPS cells infected with SARS-CoV-2 were high (Figure 3A). At the same time, ACE2 overexpression and SARS-CoV-2 infection did not alter the gene expression levels of undifferentiated markers (Figure 3B) or innate immune response-related markers (Figure 3C). The gene expression levels of endoderm markers except for *CER1* (Figure S4A) and SARS-CoV-2-related genes (*CD147*, *NRP1*, and *TMPRSS2*) (Figures S4B and 3A) were also unchanged. Immunostaining data showed that SARS-CoV-2 N protein was strongly expressed in ACE2-iPS cells 2 days after the infection (Figures 3D and S5).

We also performed an RNA sequencing (RNA-seq) analysis of uninfected and infected ACE2-iPS cells. The colored dots in the volcano plot in Figure 4A indicate genes whose expression levels changed significantly more than 4-fold. In total, this change occurred in 6.7% of all genes (Figure S6A). A GO term analysis was performed on these genes (Figures S6B and S6C). None of the genes included undifferentiated markers (Figure 4B)

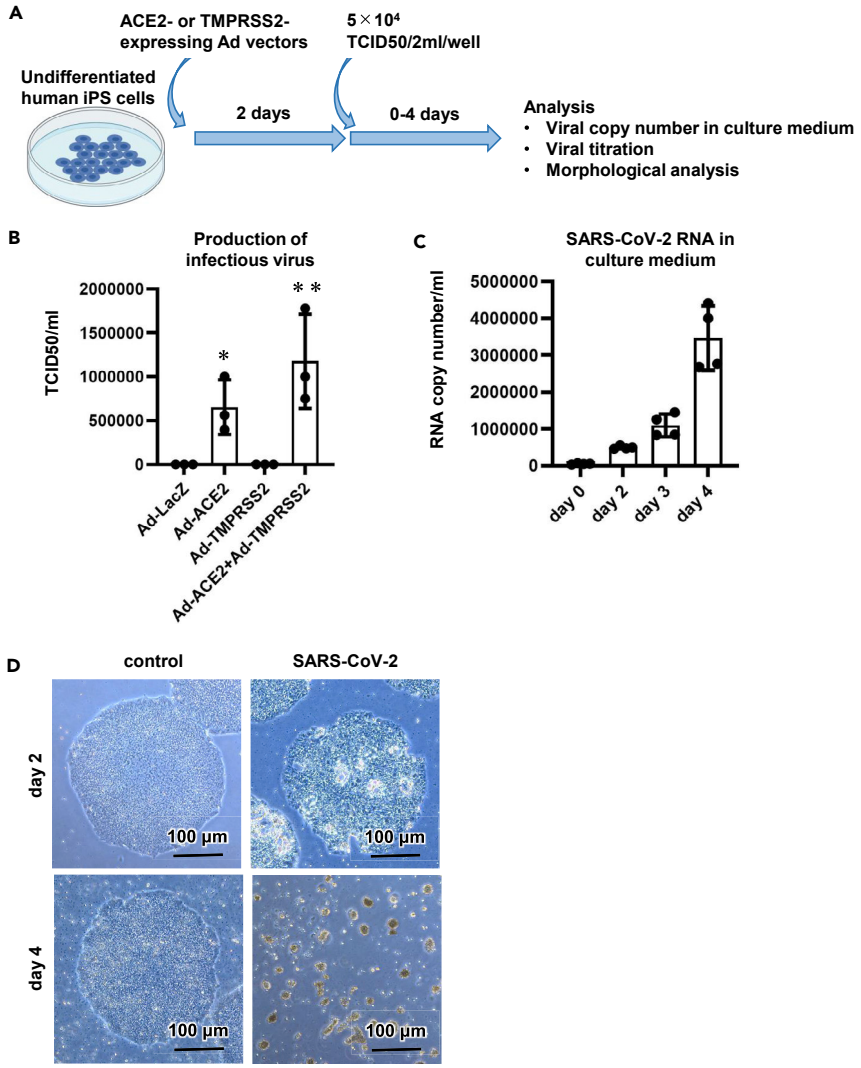

Figure 1. Efficient SARS-CoV-2 infection and replication in ACE2-iPS cells

(A) Undifferentiated human iPS cells (1383D6) were transduced with 600 vector particles (VP)/cell of LacZ-, ACE2-, or TMPRSS2-expressing Ad vectors (Ad-LacZ, Ad-ACE2, or Ad-TMPRSS2, respectively) for 2 h and then cultured with AK02 medium for 2 days. ACE2-expressing human iPS (ACE2-iPS) cells were infected with SARS-CoV-2 (5×10^4 TCID50/well) for 2 h and then cultured with AK02 medium.

(B) The amount of infectious virus in the supernatant was measured by the TCID50 assay. One-way ANOVA followed by Tukey's post hoc test (*$p < 0.05$, **$p < 0.01$, compared with Ad-LacZ).

(C) At days 0, 2, 3, and 4 after the SARS-CoV-2 infection, the viral RNA copy number in the cell culture supernatant was measured by qPCR.

(D) At days 2 and 4 after the SARS-CoV-2 infection, phase images of infected ACE2-iPS cells were obtained. Data are represented as means ± SD ($n = 3$).

See also Figures S1 and S2.

or innate immune-response markers (Figure 4C). The gene expression levels of ectoderm, mesoderm, and endoderm markers were also unchanged after infection with SARS-CoV-2 (Figure S7). Overall, these results suggest that human iPS cells maintain an undifferentiated state even when SARS-CoV-2 replicates in large numbers.

Evaluation of COVID-19 candidate drugs using ACE2-iPS cells

Next, we examined whether ACE2-iPS cells could be used for drug screening. We tried eight drugs used in COVID-19 clinical trials. Vero cells were used as the control. After exposing the cells to various concentrations of a drug, the number of viral RNA copies in the culture supernatant was quantified (Figure 5A). Data fitting

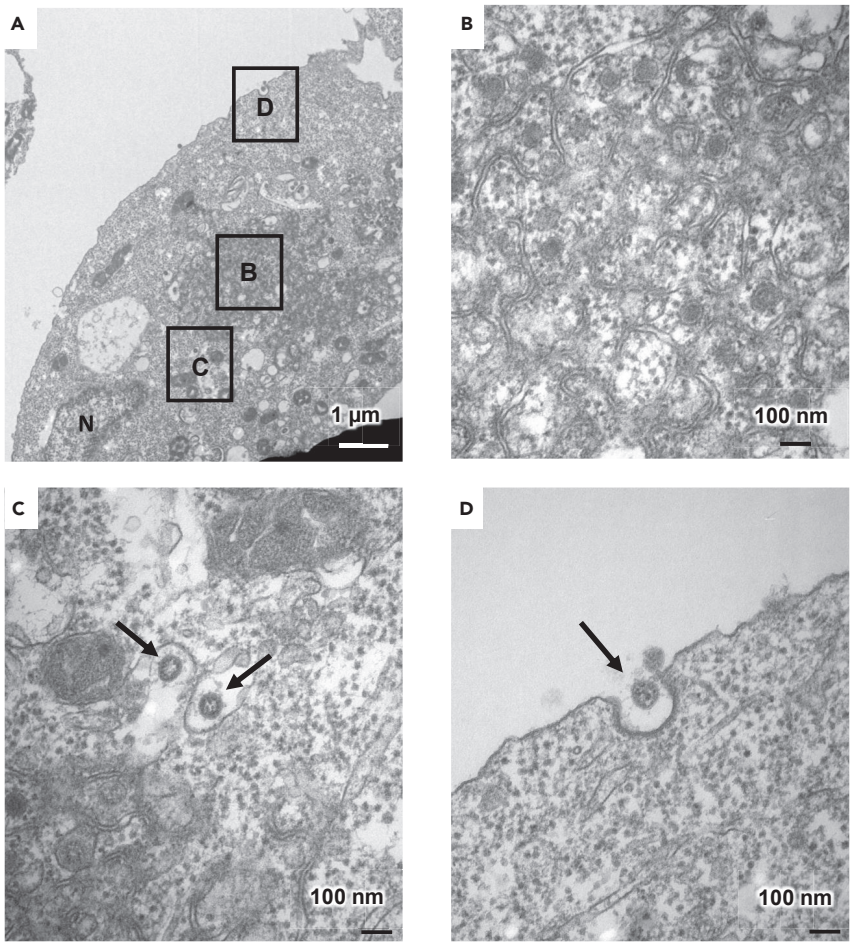

Figure 2. TEM images of infected ACE2-iPS cells

(A–D) (A) TEM images of infected ACE2-iPS cells. Zippered ER DMS (B) and virus particles in the ERGIC (black arrows) (C) and near the cell membrane (black arrows) (D) were observed.

See also Figure S3.

resulted in sigmoid curves, and half-maximal effective concentrations (EC50) were calculated (Figure 5B). Among the eight drugs, the antiviral effect of remdesivir was strongest. On the other hand, chloroquine and favipiravir did not inhibit viral replication, and ivermectin was highly cytotoxic (Figure 5C). The EC50 and half-maximal cytotoxic concentration (CC50) values of ivermectin were almost the same between control and infected ACE2-iPS cells (Figure 5D). With the exception of interferon-beta, drug effects were stronger in ACE2-iPS cells than in Vero cells. Last, we confirmed the anti-viral effects of RNA-dependent RNA polymerase (RdRp) inhibitors (remdesivir and EIDD-2801) and TMPRSS2 inhibitors (camostat and nafamostat) in ACE2-iPS cells, indicating that ACE2-iPS cells can be used to evaluate COVID-19 drug candidates.

SARS-CoV-2 infection experiments in various ACE2-iPS/ES cell lines

Finally, we performed SARS-CoV-2 infection experiments using human ACE2-iPS/ES cells established from eight donors. The replication efficiency of the virus was different among the ACE2-iPS/ES cell lines (Figure 6A). Interestingly, the viral replication capacity of male ACE2-iPS/ES cells was higher than that of female ACE2-iPS/ES cells (Figure 6B), suggesting that sex differences in the susceptibility to SARS-CoV-2 can be reproduced using ACE2-iPS/ES cells. Note that there was no significant difference in *ACE2* expression levels in the ACE2-iPS/ES cell lines (Figure 6C). Recently, it has been speculated that the expression levels of *androgen receptor* and its target gene, *TMPRSS2*, are involved in the sex differences in SARS-CoV-2 infection (Wambier et al., 2020). The *TMPRSS2* expression levels appeared to be higher in male iPS/ES cells than in female iPS/ES cells (Figure 6D), but there was no significant difference (Figure 6E).

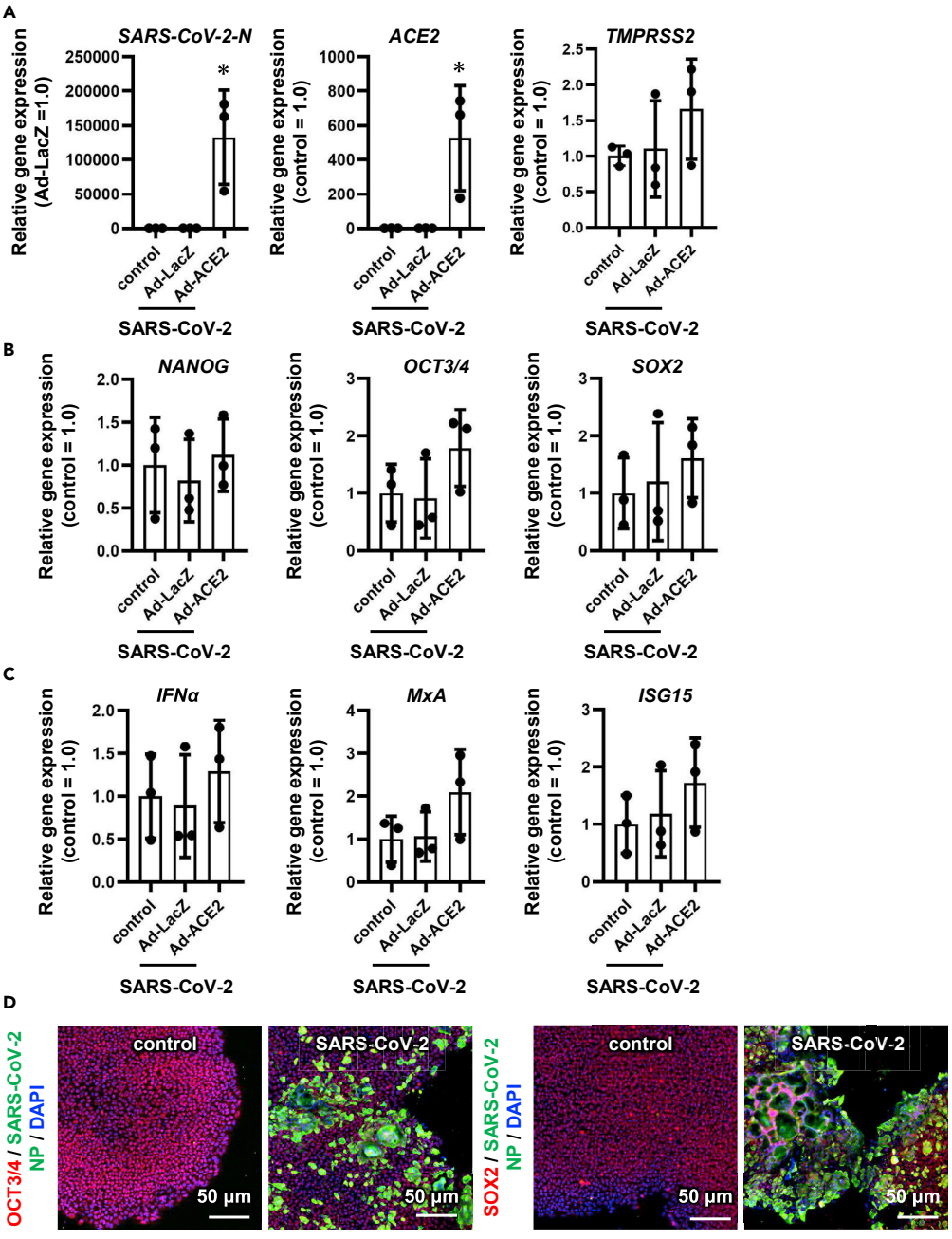

Figure 3. The pluripotent state of ACE2-iPS cells is not affected by SARS-CoV-2 infection

LacZ- or ACE2-expressing human iPS cells (LacZ-iPS cells and ACE2-iPS cells, respectively) were infected with SARS-CoV-2 (5×10^4 TCID50/well) for 2 h and then cultured with AK02 medium for 2 or 3 days. Control human iPS cells were not transduced with Ad vectors.

(A) The gene expression levels of viral genome, *ACE2*, and *TMPRSS2* were examined by qPCR analysis.

(B and C) (B) The gene expression levels of pluripotent markers (*NANOG*, *OCT3/4*, and *SOX2*) and (C) innate immunity-related markers (*IFNα*, *MxA*, and *ISG15*) were examined by qPCR.

(D) Immunofluorescence analysis of SARS-CoV-2 NP (green), OCT3/4 (red), and SOX2 (red) in uninfected and infected ACE2-iPS cells. Nuclei were counterstained with DAPI (blue). One-way ANOVA followed by Tukey's post hoc test (*$p < 0.05$, compared with Ad-LacZ). Data are represented as means ± SD ($n = 3$).

See also Figures S4 and S5, and Tables S2 and S3.

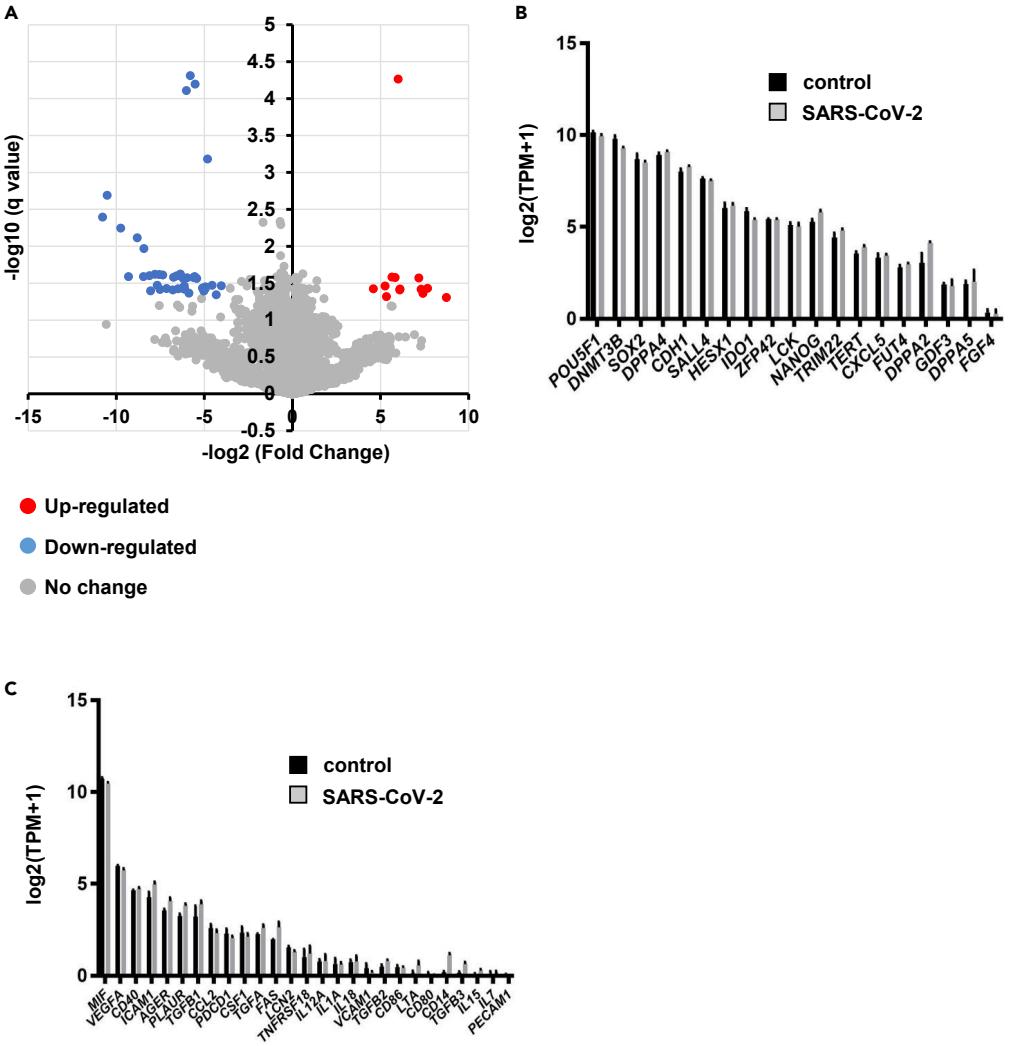

Figure 4. Global gene expression analysis of infected ACE2-iPS cells

RNA-seq analysis of uninfected or infected ACE2-iPS cells.

(A) A volcano plot of uninfected ACE2-iPS cells versus infected ACE2-iPS cells.

(B and C) Bar plots of pluripotent genes (B) and immune-related genes (C) in uninfected ACE2-iPS cells (control) and infected ACE2-iPS cells (SARS-CoV-2) are shown.

See also Figures S6 and S7.

DISCUSSION

In this study, we showed that the life cycle of SARS-CoV-2 can be reproduced in human iPS cells overexpressing ACE2. In addition, we were able to confirm the effects of two TMPRSS2 inhibitors (camostat and nafamostat) and two RdRp inhibitors (remdesivir and EIDD-2801) using these ACE2-iPS cells. Finally, we showed a difference in the efficiency of infection of SARS-CoV-2 among ACE2-iPS/ES cells from eight donors. These results suggest that by using our iPS cell panel, it will be possible to investigate the effects of race and blood type as well as gender on SARS-CoV-2 infection. By conducting SARS-CoV-2 infection experiments using a panel of iPS cells for which genomic information has been obtained, it will also be possible to find genomic mutations that appear with high frequency in susceptible cells.

We observed a difference in the infection efficiency of ACE2-iPS/ES cells between donors, but we do not know if this difference reflects the sensitivity of the original donors to COVID-19, because none were patients with COVID-19. Therefore, we are currently establishing iPS cells from patients with severe and mild COVID-19. We plan to conduct infection experiments in the newly established iPS cells and compare

A

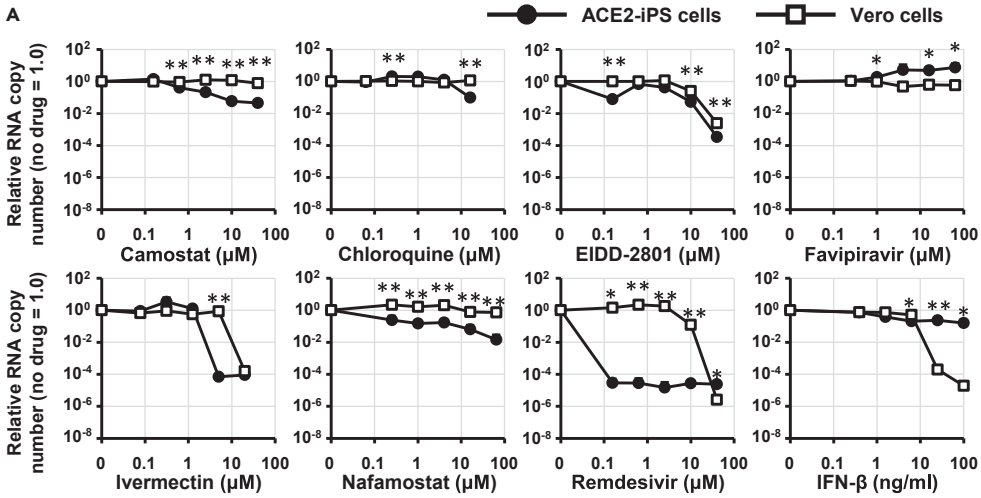

B

	Camostat	Chloroquine	EIDD-2801	Favipiravir	Ivermectin	Nafamostat	Remdesivir	IFN-β
ACE2-iPS cells	0.45 μM	-	2.14 μM	-	1.65 μM	0.046 μM	0.046 μM	0.68 ng/ml
Vero cells	-	-	8.98 μM	-	-	-	5.44 μM	8.34 ng/ml

C

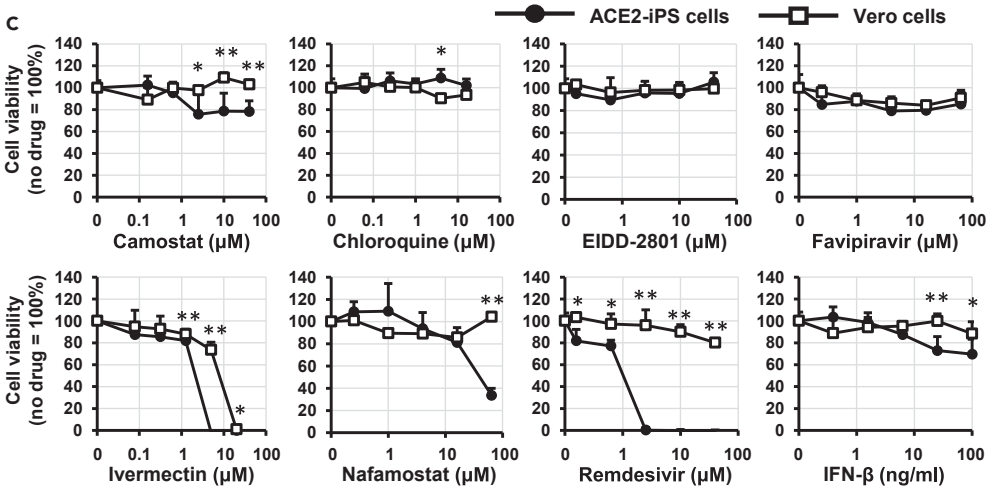

D

	Camostat	Chloroquine	EIDD-2801	Favipiravir	Ivermectin	Nafamostat	Remdesivir	IFN-β
ACE2-iPS cells	-	-	-	-	1.68 μM	34.95 μM	0.78 μM	-
Vero cells	-	-	-	-	6.98 μM	-	-	-

Figure 5. Evaluation of anti-COVID-19 drugs in ACE2-iPS cells

(A) ACE2-iPS cells and Vero cells (2.0×10^4 cells/well) were infected with SARS-CoV-2 (2.0×10^3 TCID50/well) in the presence or absence of a drug and then cultured with medium for 4 and 2 days, respectively. The viral RNA copy number in the cell culture supernatant was measured by qPCR.

(B) The EC50 values (μM) of anti-COVID-19 drugs in ACE2-iPS cells and Vero cells were calculated using GraphPad Prism8 and are summarized.

(C) Vero cells and ACE2-iPS cells were cultured with medium containing drugs for 4 days. Cell viability was measured by the WST-8 assay.

(D) The CC50 values (μM) of anti-COVID-19 drugs in Vero cells and ACE2-iPS cells were calculated using GraphPad Prism8 and summarized. Data are represented as means ± SD ($n = 3$). Unpaired two-tailed Student's t test (*$p < 0.05$, **$p < 0.01$; ACE2-iPS versus Vero cells).

See also Table S1.

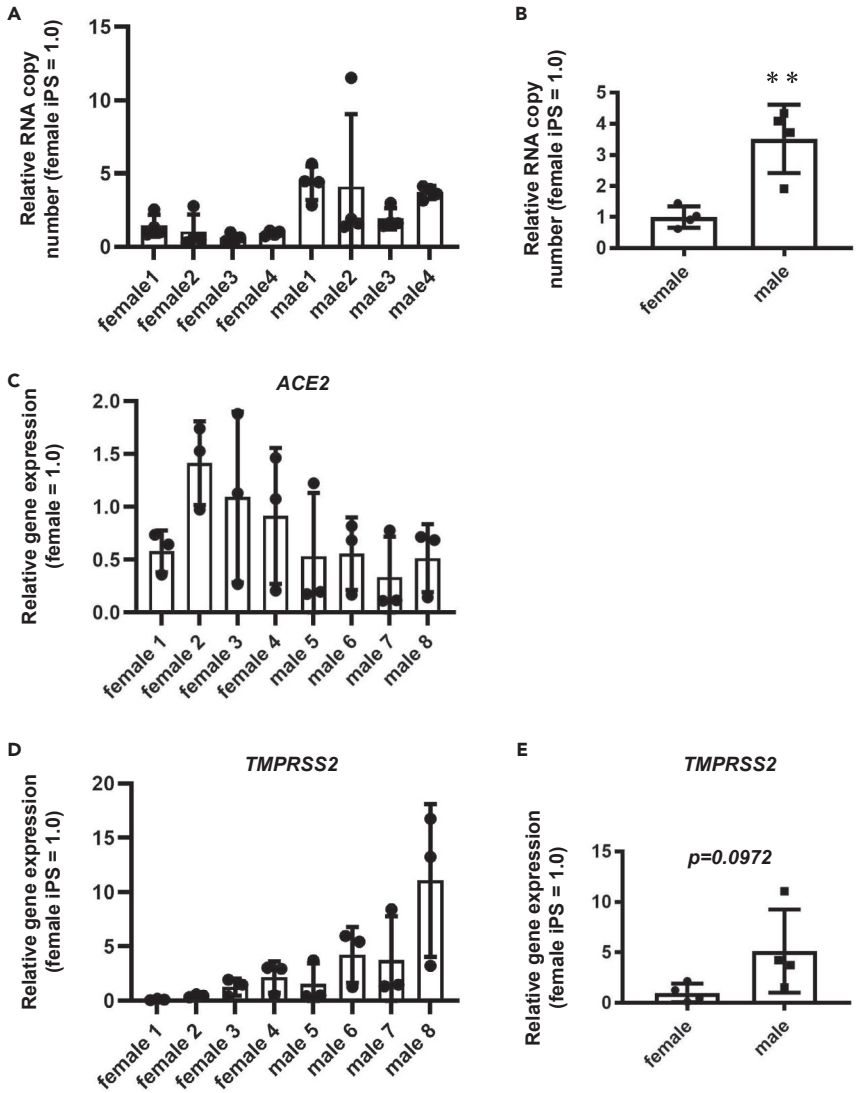

Figure 6. Sex differences of the SARS-CoV-2 infection rate in ACE2-ES/iPS cells

Four female ES/iPS cell lines and four male ES/iPS cell lines were transduced with 600 VP/cell of ACE2-expressing Ad vectors (Ad-ACE2) for 2 h and then cultured with AK02 medium for 2 days. The cells were then infected with SARS-CoV-2 (5×10^4 TCID50/well) for 2 h and cultured with AK02 medium.

(A) The viral RNA copy number in the cell culture supernatant was measured by qPCR for each cell line.

(B) The viral RNA copy number in the cell culture supernatant was compared between female iPS/ES cells and male iPS/ES cells.

(C and D) *ACE2* (C) and *TMPRSS2* (D) expression levels were measured by qPCR for each cell line.

(E) *TMPRSS2* expression levels were compared between female iPS/ES cells and male iPS/ES cells. Unpaired two-tailed Student's t test (**$p < 0.01$). Data are represented as means ± SD ($n = 3$). Female 1: H9, Female 2: KhES1, Female 3: KhES2, Female 4: 201B7, Male 1: H1, Male 2: KhES3, Male 3: Tic, Male 4: 1383D6.

See also Table S2.

the results with the symptoms of the original patients. These experiments could clarify whether the results of SARS-CoV-2 infection experiments using iPS cells reflect the symptoms of the original donors.

In this study, we confirmed sex differences in the susceptibility to SARS-CoV-2. Testosterone is known as a ligand for the androgen receptor, which regulates the expression of TMPRSS2 (Wambier et al., 2020). By generating iPS cell-derived Leydig cells that are capable of producing testosterone (Li et al., 2019), more prominent sex differences in the susceptibility to SARS-CoV-2 may be confirmed. Thus, ACE2-iPS cells and differentiated cells may have different susceptibility to SARS-CoV-2. In the future, it is expected

that more accurate results will be obtained by conducting infection experiments using ACE2-iPS cells and differentiated cells at the same time.

Recently, GWAS analyses were performed on patients with severe and mild COVID-19 (Group, 2020; Pairo-Castineira et al., 2021). The analysis of the severe COVID-19 GWAS group indicated that mutations in the SLC6A20, LZTFL1, CCR9, FYCO1, CXCR6, and XCR1 genes are associated with the severity of the symptoms (Group, 2020). Pairo-Castineira et al. suggested that the mutations and expression levels of the IFNAR2 and TYK2 genes are also associated with the severity of COVID-19 (Pairo-Castineira et al., 2021). However, the function of these genes in COVID-19 is still not fully understood. Further analysis can be performed by examining the relationship between viral infection and gene mutations and expressions in our iPS cell panel. Because single-nucleotide mutations can be easily introduced into iPS cells (Kim et al., 2018), the function of these mutations can be studied using genome-edited iPS cells.

Accordingly, there may be multiple causes of the individual differences in COVID-19 symptoms. The ACE2-iPS cells that we have developed in this study will be one tool to elucidate the cause of these individual differences, which will help identify vulnerable populations and develop new drugs.

Limitations of the study

To infect iPS cells with SARS-CoV-2, we overexpressed ACE2. However, if ACE2 and its related genes are responsible for the individual differences in SARS-CoV-2 infection, our system will not be effective. To analyze the mutation and expression of ACE2 and its related genes, it is essential to use somatic cells expressing ACE2. Also, our system is not effective for studying the non-genetic causes of individual differences in COVID-19 severity. For example, it has been speculated that age-related differences in COVID-19 symptoms are due to impaired cytotoxic CD8+ T cell responses (Westmeier et al., 2020). For such studies, it is more suitable to use blood samples.

Resource availability

Lead contact

Dr. Kazuo Takayama.

Center for iPS Cell Research and Application, Kyoto University, Shogoin Kawaharacho 53, Sakyo-ku, Kyoto 606-8397, Japan.

Phone: +81-75-366-7362, FAX: +81-75-366-7074.

E-mail: kazuo.takayama@cira.kyoto-u.ac.jp.

Materials availability

All unique/stable reagents generated in this study are available from the corresponding authors with a completed Materials Transfer Agreement.

Data and code availability

Raw data of RNA-seq analysis were submitted under Gene Expression Omnibus (GEO) accession number GSE166990.

METHODS

All methods can be found in the accompanying Transparent methods supplemental file.

SUPPLEMENTAL INFORMATION

Supplemental information can be found online at https://doi.org/10.1016/j.isci.2021.102428.

ACKNOWLEDGMENTS

The SARS-CoV-2 strain used in this study (SARS-CoV-2/Hu/DP/Kng/19-027) was kindly provided by Dr. Tomohiko Takasaki and Dr. Jun-Ichi Sakuragi (Kanagawa Prefectural Institute of Public Health). Figures 1A and S1A were created using Biorender (https://biorender.com). We thank Dr. Misaki Ouchida (Kyoto University) for creating the graphical abstract, Dr. Peter Karagiannis (Kyoto University) for critical reading of the manuscript; Dr. Masato

Nagagawa (Kyoto University) for providing the human iPS cells; Dr. Yoshio Koyanagi and Dr. Kazuya Shimura (Kyoto University) for the setup and operation of the BSL-3 laboratory at Kyoto University; Dr. Toru Okamoto (Osaka University), Dr. Akatsuki Saito (University of Miyazaki), Dr. Hirofumi Ohashi, and Dr. Koichi Watashi (National Institute of Infectious Diseases) for helpful discussion; and Ms. Kazusa Okita and Ms. Satoko Sakurai (Kyoto University) for technical assistance with the RNA-seq experiments. This research was supported by the iPS Cell Research Fund, the COVID-19 Private Fund (to the Shinya Yamanaka laboratory, CiRA, Kyoto University), the Joint Usage/Research Center program of Institute for Frontier Life and Medical Sciences, Kyoto University, the Astellas Foundation for Research on Metabolic Disorders, the Senri Life Science Foundation, the Mitsubishi Foundation, the JST Core Research for Evolutional Science and Technology (JPMJCR20HA), and the Japan Agency for Medical Research and Development (AMED) (20fk0108263s0201, 20fk0108518s0401, 20fk0108511h0201).

AUTHOR CONTRIBUTIONS

E.S. performed the SARS-CoV-2 experiments, analyses, and statistical analysis. S.D. performed the data analysis and statistical analysis. A.S. performed the human cell culture and qPCR analyses. N.M. performed the drug experiments. A.H. obtained the TEM images. Y.M. obtained the TEM images. T.N. obtained the TEM images. T.Y. performed the RNA-seq analysis. K.T. performed the SARS-CoV-2 experiments and analyses and wrote the paper.

DECLARATION OF INTERESTS

The authors declare no competing financial interests.

Received: March 2, 2021
Revised: March 19, 2021
Accepted: April 9, 2021
Published: May 21, 2021

REFERENCES

Anastassopoulou, C., Gkizarioti, Z., Patrinos, G.P., and Tsakris, A. (2020). Human genetic factors associated with susceptibility to SARS-CoV-2 infection and COVID-19 disease severity. Hum. Genomics *14*, 1–8.

Group, S.C.-G. (2020). Genomewide association study of severe Covid-19 with respiratory failure. New Engl. J. Med. *383*, 1522–1534.

Han, Y., Duan, X., Yang, L., Nilsson-Payant, B.E., Wang, P., Duan, F., Tang, X., Yaron, T.M., Zhang, T., and Uhl, S. (2021). Identification of SARS-CoV-2 inhibitors using lung and colonic organoids. Nature *589*, 270–275.

Hoffmann, M., Kleine-Weber, H., Schroeder, S., Krüger, N., Herrler, T., Erichsen, S., Schiergens, T.S., Herrler, G., Wu, N.-H., and Nitsche, A. (2020). SARS-CoV-2 cell entry depends on ACE2 and TMPRSS2 and is blocked by a clinically proven protease inhibitor. Cell *181*, 271–280. e278.

Kajiwara, M., Aoi, T., Okita, K., Takahashi, R., Inoue, H., Takayama, N., Endo, H., Eto, K., Toguchida, J., and Uemoto, S. (2012). Donor-dependent variations in hepatic differentiation from human-induced pluripotent stem cells. Proc. Natl. Acad. Sci. U S A *109*, 12538–12543.

Kim, S.-I., Matsumoto, T., Kagawa, H., Nakamura, M., Hirohata, R., Ueno, A., Ohishi, M., Sakuma, T., Soga, T., and Yamamoto, T. (2018). Microhomology-assisted scarless genome editing in human iPSCs. Nat. Commun. *9*, 1–14.

Klein, S., Cortese, M., Winter, S.L., Wachsmuth-Melm, M., Neufeldt, C.J., Cerikan, B., Stanifer, M.L., Boulant, S., Bartenschlager, R., and Chlanda, P. (2020). SARS-CoV-2 structure and replication characterized by in situ cryo-electron tomography. Nat. Commun. *11*, 1–10.

Li, L., Li, Y., Sottas, C., Culty, M., Fan, J., Hu, Y., Cheung, G., Chemes, H.E., and Papadopoulos, V. (2019). Directing differentiation of human induced pluripotent stem cells toward androgen-producing Leydig cells rather than adrenal cells. Proc. Natl. Acad. Sci. U S A *116*, 23274–23283.

Maier, H.J., Hawes, P.C., Cottam, E.M., Mantell, J., Verkade, P., Monaghan, P., Wileman, T., and Britton, P. (2013). Infectious bronchitis virus generates spherules from zippered endoplasmic reticulum membranes. mBio *4*, e00801–13.

Pairo-Castineira, E., Clohisey, S., Klaric, L., Bretherick, A.D., Rawlik, K., Pasko, D., Walker, S., Parkinson, N., Fourman, M.H., and Russell, C.D. (2021). Genetic mechanisms of critical illness in Covid-19. Nature *591*, 92–98.

Park, I.-H., Arora, N., Huo, H., Maherali, N., Ahfeldt, T., Shimamura, A., Lensch, M.W., Cowan, C., Hochedlinger, K., and Daley, G.Q. (2008). Disease-specific induced pluripotent stem cells. Cell *134*, 877–886.

Takahashi, K., Tanabe, K., Ohnuki, M., Narita, M., Ichisaka, T., Tomoda, K., and Yamanaka, S. (2007). Induction of pluripotent stem cells from adult human fibroblasts by defined factors. Cell *131*, 861–872.

Takayama, K. (2020). In vitro and animal models for SARS-CoV-2 research. Trends Pharmacol. Sci. *41*, 513–517.

Wambier, C.G., Goren, A., Vaño-Galván, S., Ramos, P.M., Ossimetha, A., Nau, G., Herrera, S., and McCoy, J. (2020). Androgen sensitivity gateway to COVID-19 disease severity. Drug Dev. Res. *81*, 771–776.

Wang, K., Chen, W., Zhang, Z., Deng, Y., Lian, J.-Q., Du, P., Wei, D., Zhang, Y., Sun, X.-X., and Gong, L. (2020). CD147-spike protein is a novel route for SARS-CoV-2 infection to host cells. Signal Transduct. Target. Ther. *5*, 1–10.

Weiss, P., and Murdoch, D.R. (2020). Clinical course and mortality risk of severe COVID-19. Lancet *395*, 1014–1015.

Westmeier, J., Paniskaki, K., Karaköse, Z., Werner, T., Sutter, K., Dolff, S., Overbeck, M., Limmer, A., Liu, J., and Zheng, X. (2020). Impaired cytotoxic CD8+ T cell response in elderly COVID-19 patients. mBio *11*, e02243–20.

Zeberg, H., and Pääbo, S. (2020). The major genetic risk factor for severe COVID-19 is inherited from Neanderthals. Nature *587*, 610–612.

Ziegler, C.G., Allon, S.J., Nyquist, S.K., Mbano, I.M., Miao, V.N., Tzouanas, C.N., Cao, Y., Yousif, A.S., Bals, J., and Hauser, B.M. (2020). SARS-CoV-2 receptor ACE2 is an interferon-stimulated gene in human airway epithelial cells and is detected in specific cell subsets across tissues. Cell *181*, 1016–1035. e1019.

iScience, Volume *24*

Supplemental information

Modeling SARS-CoV-2 infection and its individual differences with ACE2-expressing human iPS cells

Emi Sano, Sayaka Deguchi, Ayaka Sakamoto, Natsumi Mimura, Ai Hirabayashi, Yukiko Muramoto, Takeshi Noda, Takuya Yamamoto, and Kazuo Takayama

Supplemental figures

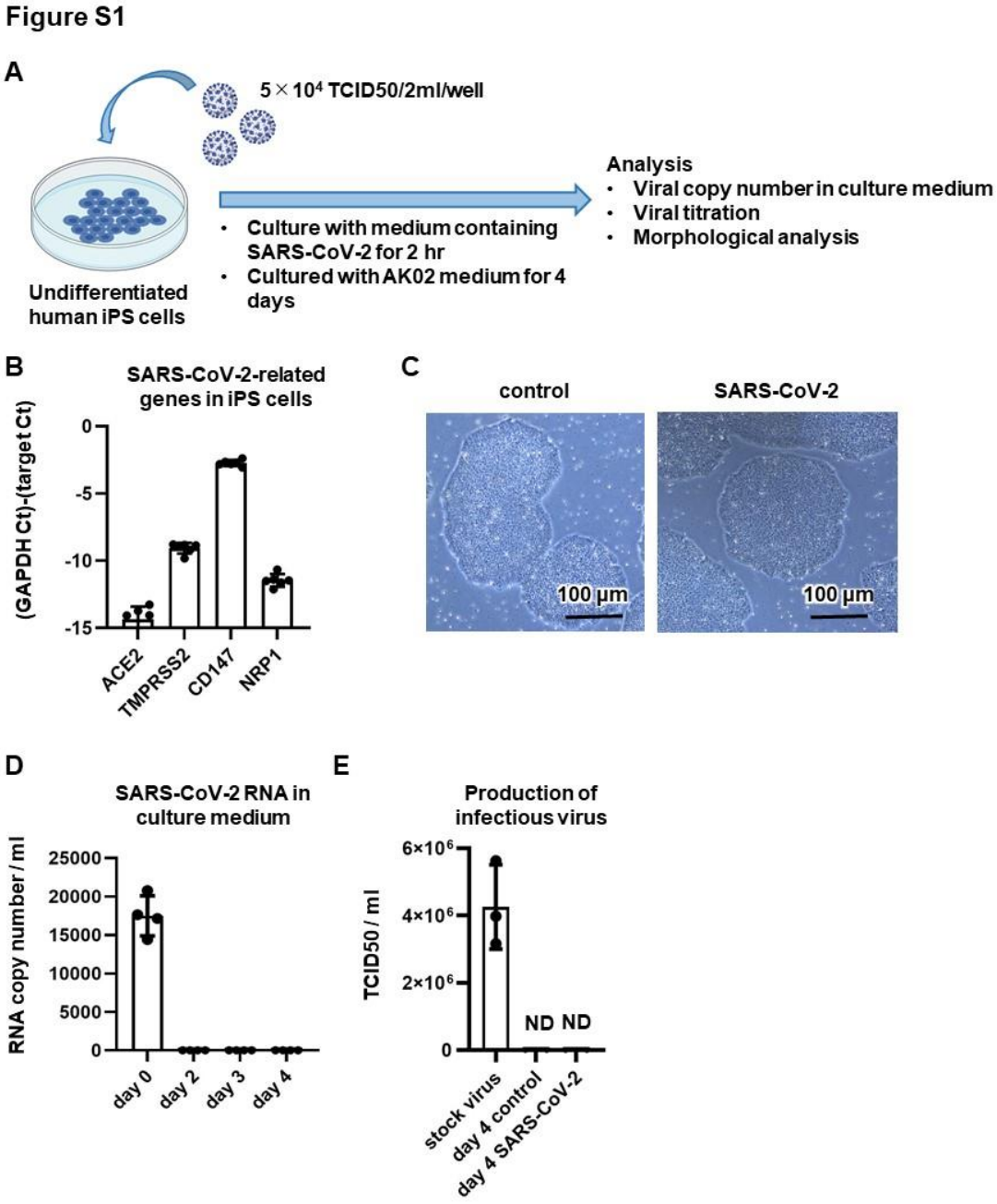

Figure S1 SARS-CoV-2 cannot infect human iPS cells, Related to Figure 1

(**A**) Undifferentiated human iPS cells (1383D6) were infected with SARS-CoV-2 (5×10^4 TCID50/well) for 2 hr and then cultured with AK02 medium for 4 days. (**B**) The gene expression levels of *ACE2*, *TMPRSS2*, *CD147*, and *NRP1* in human iPS cells were examined by qPCR. (**C**) Phase images of uninfected and infected human iPS cells are shown. (**D**) At days 0, 2, 3 and 4 after the infection, the viral RNA copy number in the

cell culture supernatant was measured by qPCR. day 0 = medium containing initial virus (5×104 TCID50/2ml). (**E**) The amount of infectious virus in the supernatant was measured by the TCID50 assay. Data are represented as means ± SD (*n*=3). ND=not detected.

Figure S2

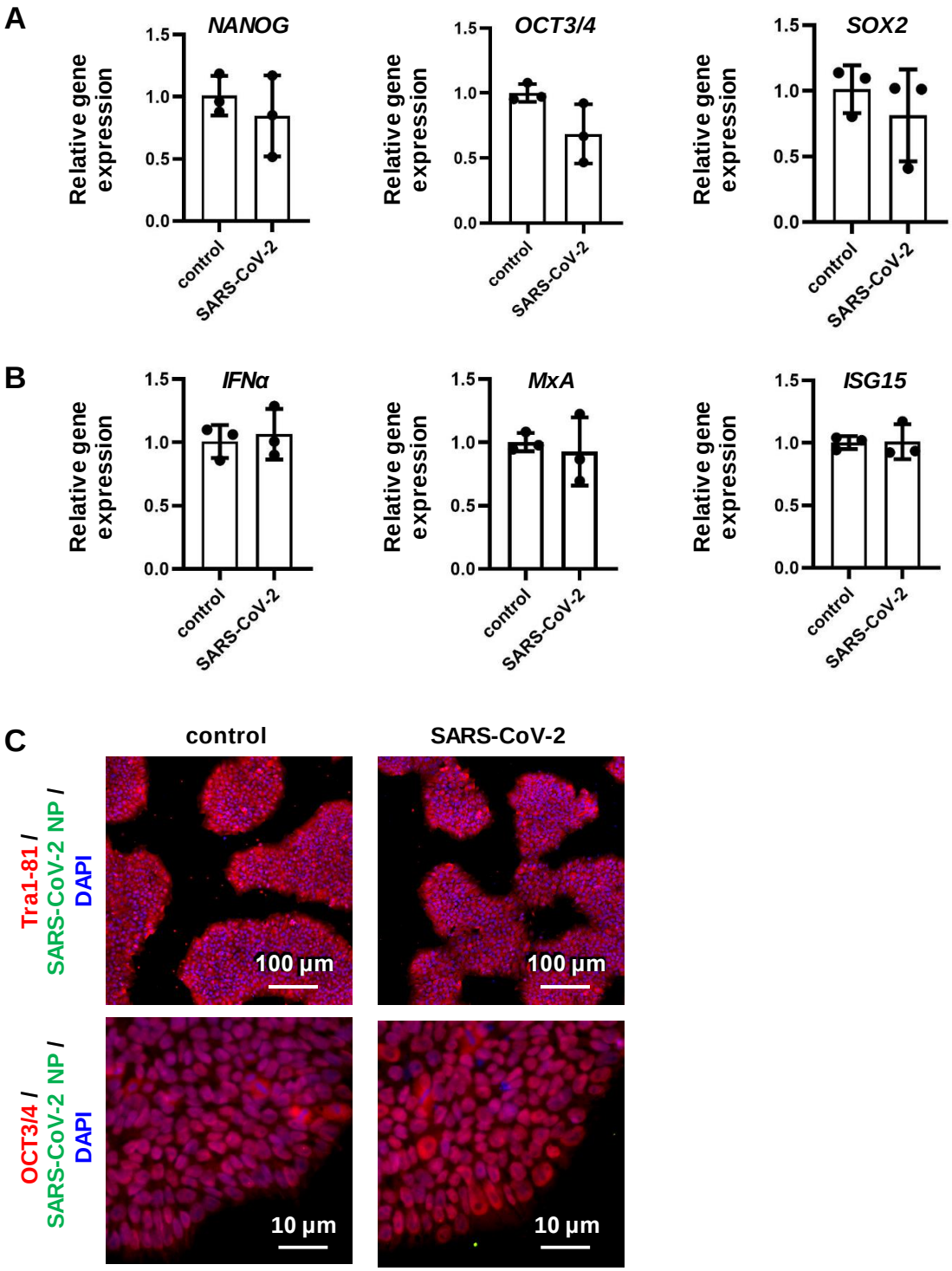

Figure S2 The pluripotent state of human iPS cells is not affected by SARS-CoV-2 infection, Related to Figure 1

The gene expression levels of pluripotent markers (*NANOG*, *OCT3/4*, and *SOX2*) (**A**) and innate immunity-related markers (*IFNα*, *MxA*, and *ISG15*) (**B**) in uninfected and infected human iPS cells were examined by qPCR. (**C**) Immunofluorescence analysis of SARS-CoV-2 NP (green), Tra1-81 (red), and OCT3/4 (red) in uninfected and infected human iPS cells. Nuclei were counterstained with DAPI (blue). Data are represented as means ± SD (*n*=3).

Figure S3

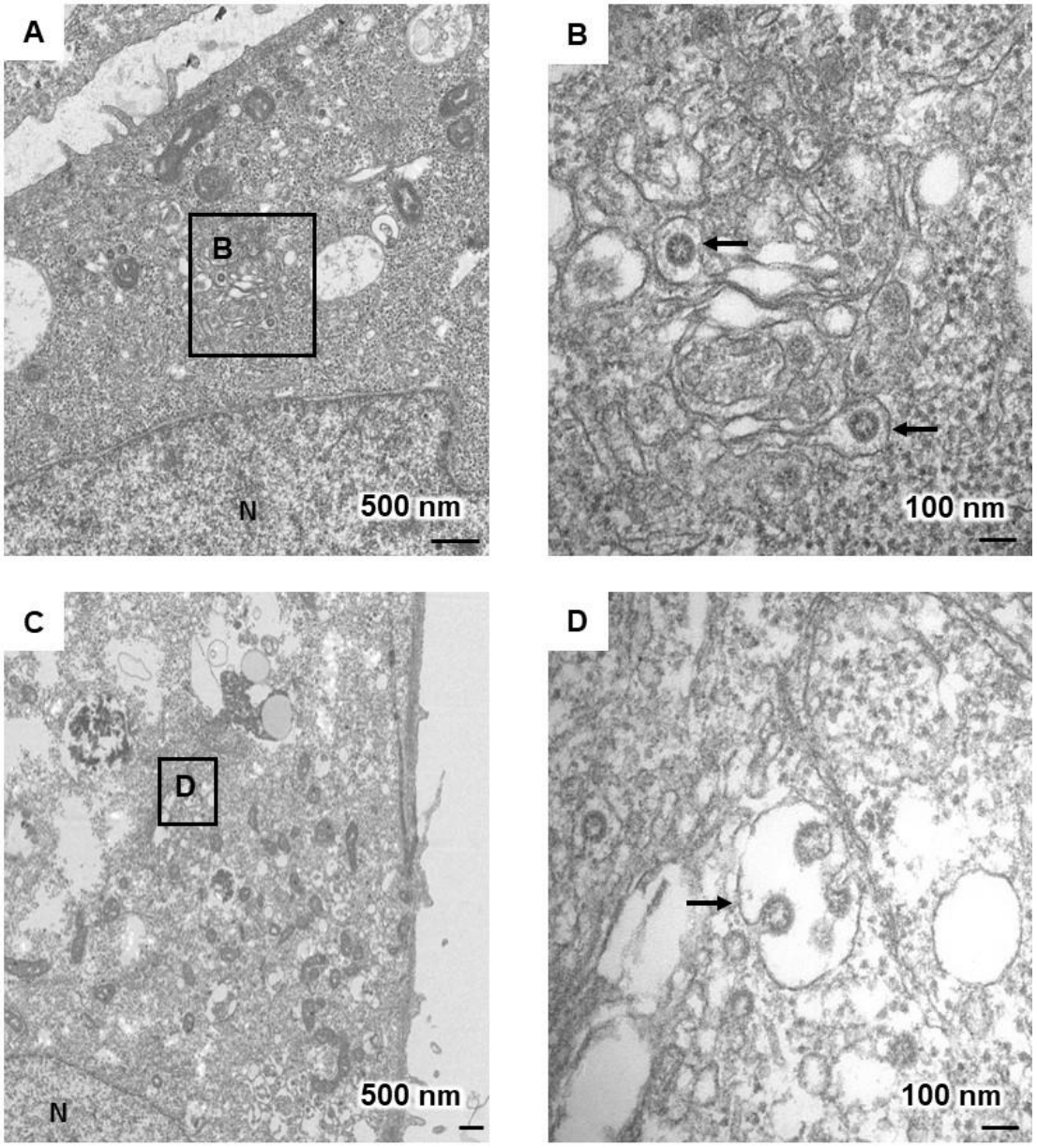

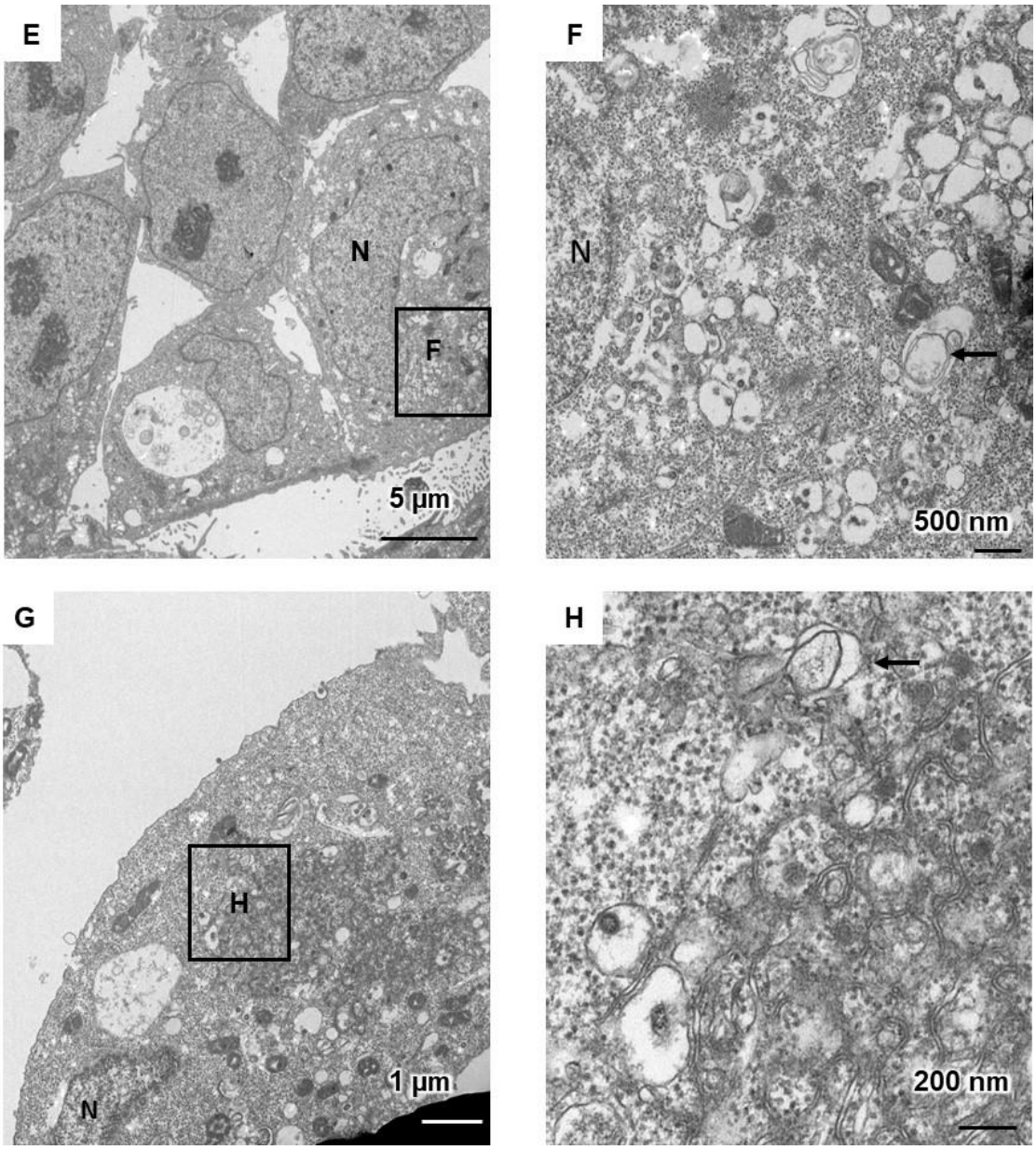

Figure S3　TEM images of infected ACE2-iPS cells, Related to Figure 2

(**A-D**) Endoplasmic reticulum-Golgi intermediate compartment (ERGIC) containing SARS-CoV-2 particles (black arrows) was observed in infected ACE2-iPS cells. (**E-H**) Double membrane vesicles (black arrows) were observed in infected ACE2-iPS cells.

Figure S4

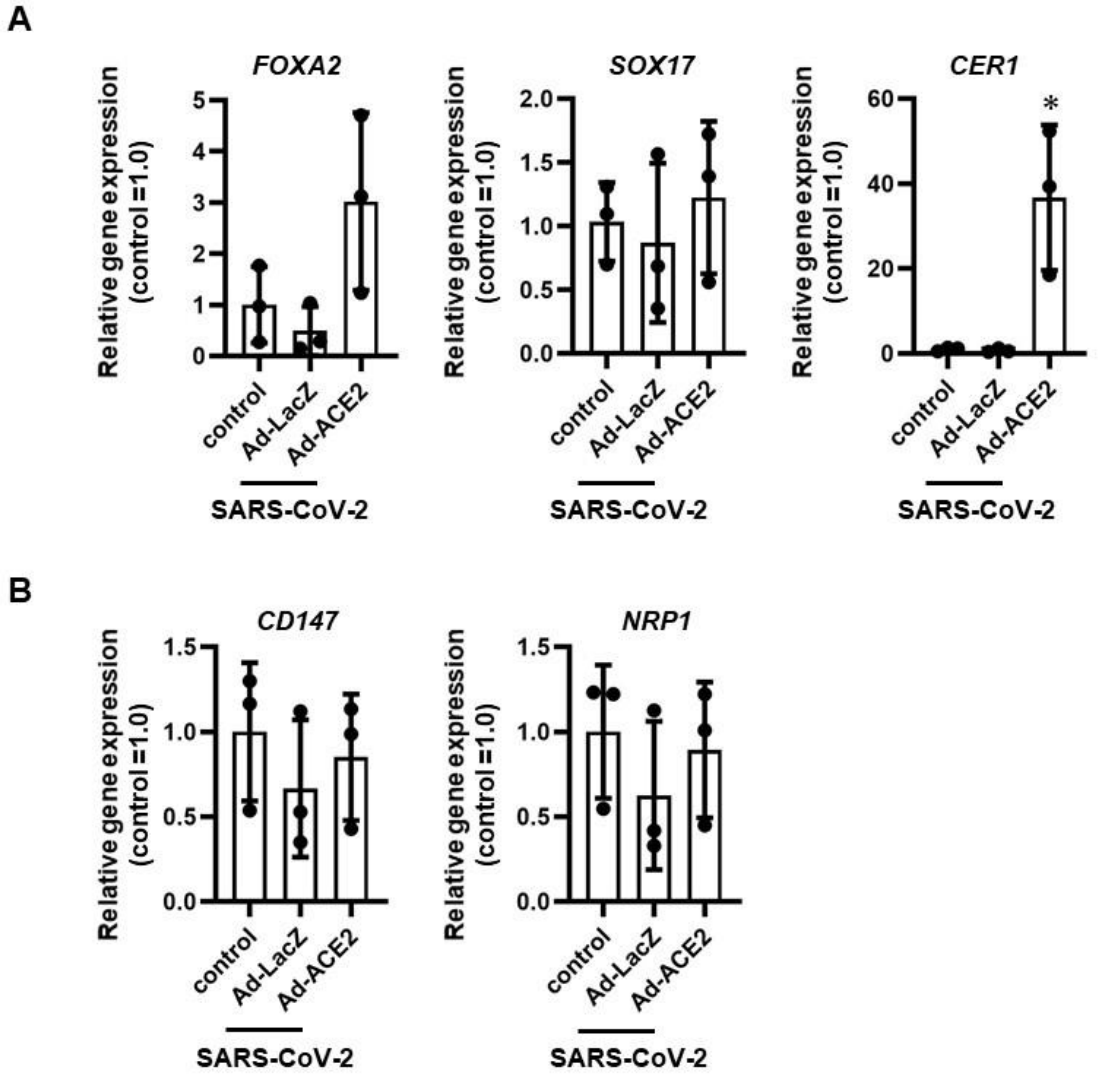

Figure S4　Gene expression profiles of differentiation markers and viral receptors in infected ACE2-iPS cells, Related to Figure 3

Undifferentiated human iPS cells (1383D6) were transduced with 600 VP/cell of LacZ- or ACE2-expressing Ad vectors (Ad-LacZ and Ad-ACE2, respectively) for 2 hr and then cultured with AK02 medium for 2 days. Control human iPS cells were not transduced with Ad vectors. The LacZ- and ACE2-expressing human iPS cells were then infected with SARS-CoV-2 (5×10^4 TCID50/well) for 2 hr and cultured with AK02 medium for 3 days. (**A, B**) The gene expression levels of endoderm markers (*FOXA2*, *SOX17*, and *CER1*) (**A**) and viral receptors (*CD147* and *NRP1*) (**B**) were examined by qPCR. Data are represented as means ± SD (n=3). One-way ANOVA followed by Tukey's post hoc test (*p<0.05, compared with Ad-LacZ).

Figure S5

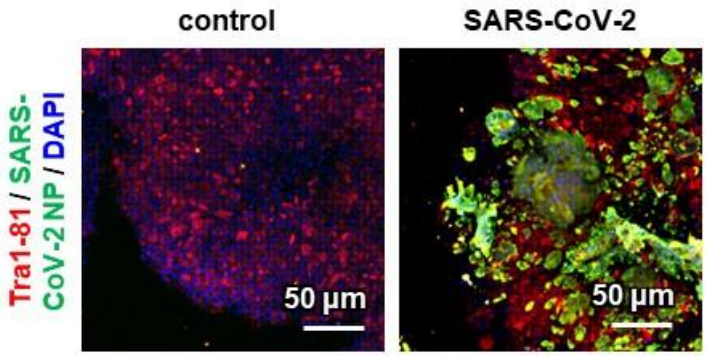

Figure S5　Immunofluorescence analysis of infected ACE2-iPS cells, Related to Figure 3

Immunofluorescence analysis of SARS-CoV-2 NP (green) and OCT3/4 (red) in uninfected and infected ACE2-iPS cells. Nuclei were counterstained with DAPI (blue).

Figure S6

A

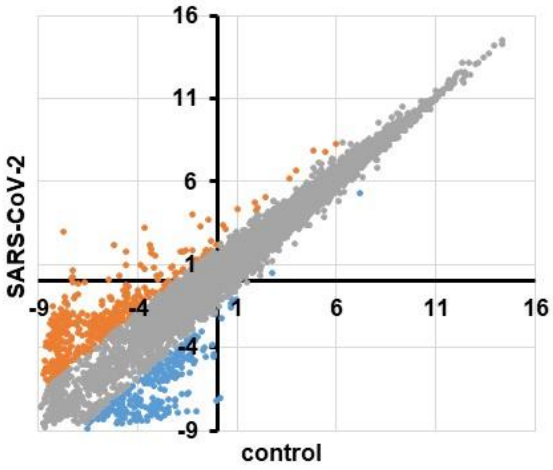

Dot	Description	Count	Rate (%)
	Detected	19370	
●	Up-regulated	792	4.1
●	Down-regulated	494	2.6
●	No change	18084	93.4

B

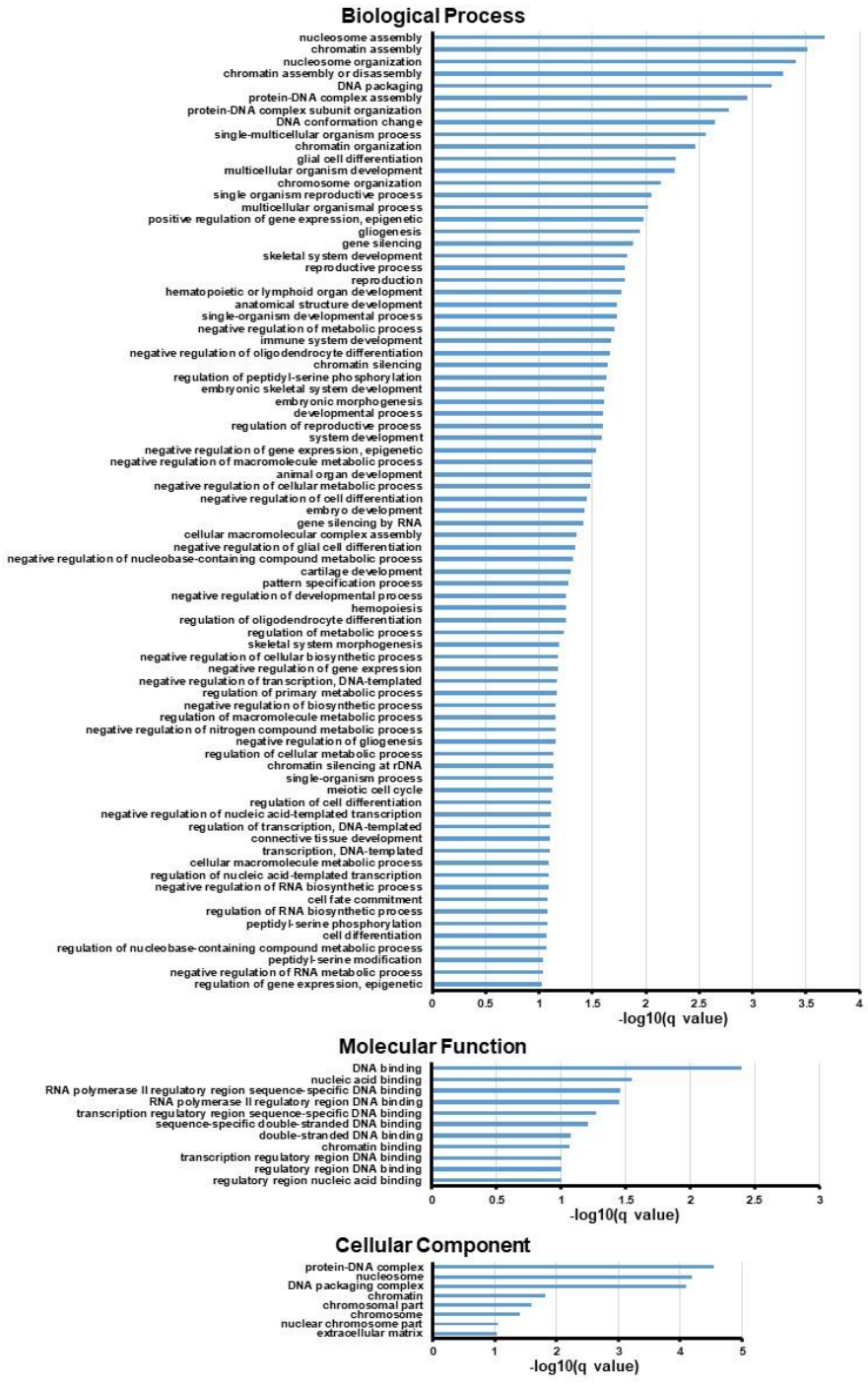
Biological Process
nucleosome assembly
chromatin assembly
nucleosome organization
chromatin assembly or disassembly
DNA packaging
protein-DNA complex assembly
protein-DNA complex subunit organization
DNA conformation change
single-multicellular organism process
chromatin organization
glial cell differentiation
multicellular organism development
chromosome organization
single organism reproductive process
multicellular organismal process
positive regulation of gene expression, epigenetic
gliogenesis
gene silencing
skeletal system development
reproductive process
reproduction
hematopoietic or lymphoid organ development
anatomical structure development
single-organism developmental process
negative regulation of metabolic process
immune system development
negative regulation of oligodendrocyte differentiation
chromatin silencing
regulation of peptidyl-serine phosphorylation
embryonic skeletal system development
embryonic morphogenesis
developmental process
regulation of reproductive process
system development
negative regulation of gene expression, epigenetic
negative regulation of macromolecule metabolic process
animal organ development
negative regulation of cellular metabolic process
negative regulation of cell differentiation
embryo development
gene silencing by RNA
cellular macromolecular complex assembly
negative regulation of glial cell differentiation
negative regulation of nucleobase-containing compound metabolic process
cartilage development
pattern specification process
negative regulation of developmental process
hemopoiesis
regulation of oligodendrocyte differentiation
regulation of metabolic process
skeletal system morphogenesis
negative regulation of cellular biosynthetic process
negative regulation of gene expression
negative regulation of transcription, DNA-templated
regulation of primary metabolic process
negative regulation of biosynthetic process
regulation of macromolecule metabolic process
negative regulation of nitrogen compound metabolic process
negative regulation of gliogenesis
regulation of cellular metabolic process
chromatin silencing at rDNA
single-organism process
meiotic cell cycle
regulation of cell differentiation
negative regulation of nucleic acid-templated transcription
regulation of transcription, DNA-templated
connective tissue development
transcription, DNA-templated
cellular macromolecule metabolic process
regulation of nucleic acid-templated transcription
negative regulation of RNA biosynthetic process
cell fate commitment
regulation of RNA biosynthetic process
peptidyl-serine phosphorylation
cell differentiation
regulation of nucleobase-containing compound metabolic process
peptidyl-serine modification
negative regulation of RNA metabolic process
regulation of gene expression, epigenetic
0
0.5
1
1.5
2
2.5
3
3.5
4
-log10(q value)
Molecular Function
DNA binding
nucleic acid binding
RNA polymerase II regulatory region sequence-specific DNA binding
RNA polymerase II regulatory region DNA binding
transcription regulatory region sequence-specific DNA binding
sequence-specific double-stranded DNA binding
double-stranded DNA binding
chromatin binding
transcription regulatory region DNA binding
regulatory region DNA binding
regulatory region nucleic acid binding
0
0.5
1
1.5
2
2.5
3
-log10(q value)
Cellular Component
protein-DNA complex
nucleosome
DNA packaging complex
chromatin
chromosomal part
chromosome
nuclear chromosome part
extracellular matrix
0
1
2
3
4
5
-log10(q value)

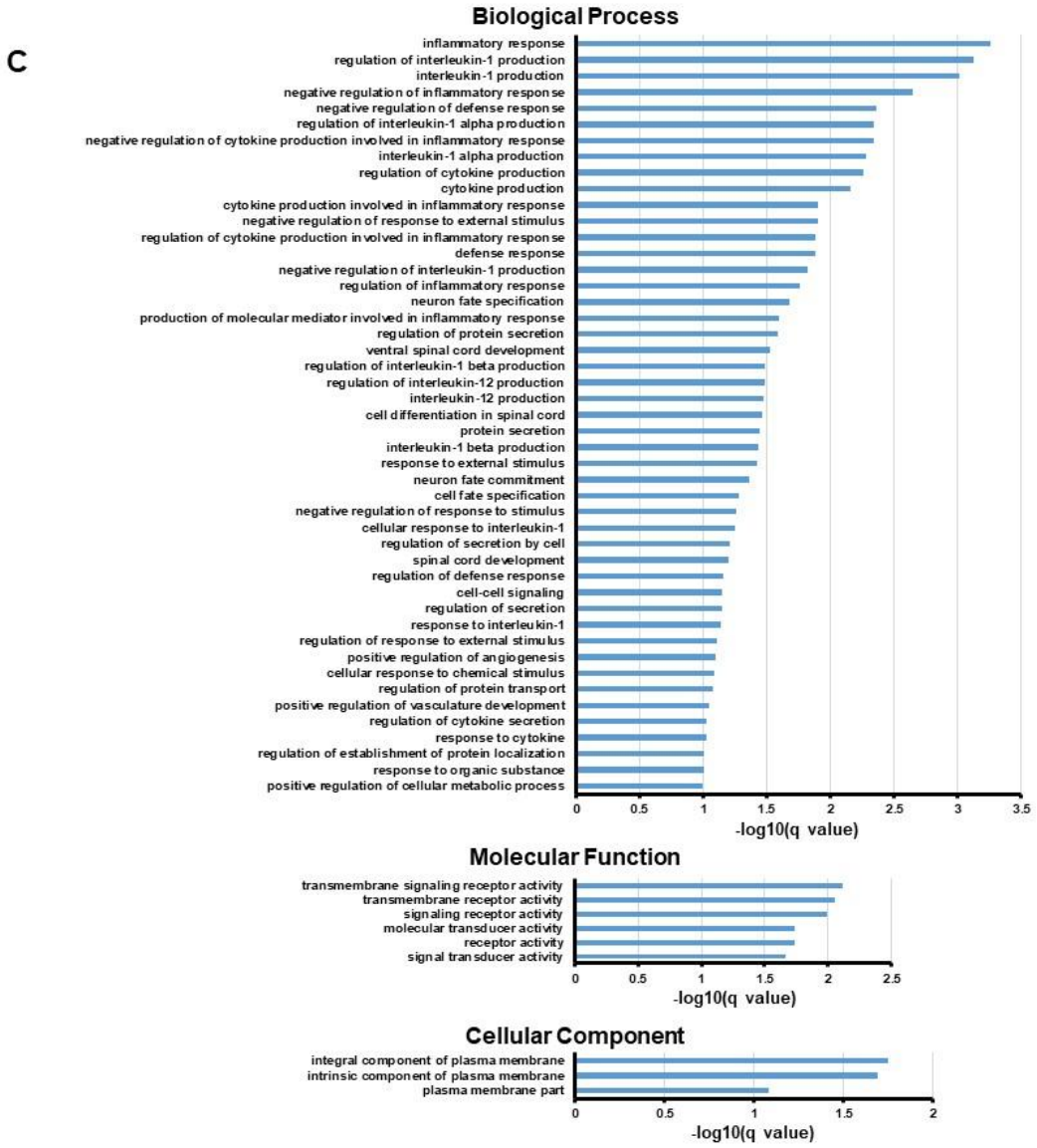

Figure S6　Global gene expression analysis of infected ACE2-iPS cells, Related to Figure 4

RNA-seq analysis of uninfected and infected ACE2-iPS cells. (**A**) A scatter plot of uninfected ACE2-iPS cells (control) vs. infected ACE2-iPS cells (SARS-CoV-2). The count and rate of up-regulated and down-regulated genes are summarized in the table. (**B, C**) GO analysis was performed for gene sets whose gene expression levels were decreased (**B**) or increased (**C**) more than three-fold.

Figure S7

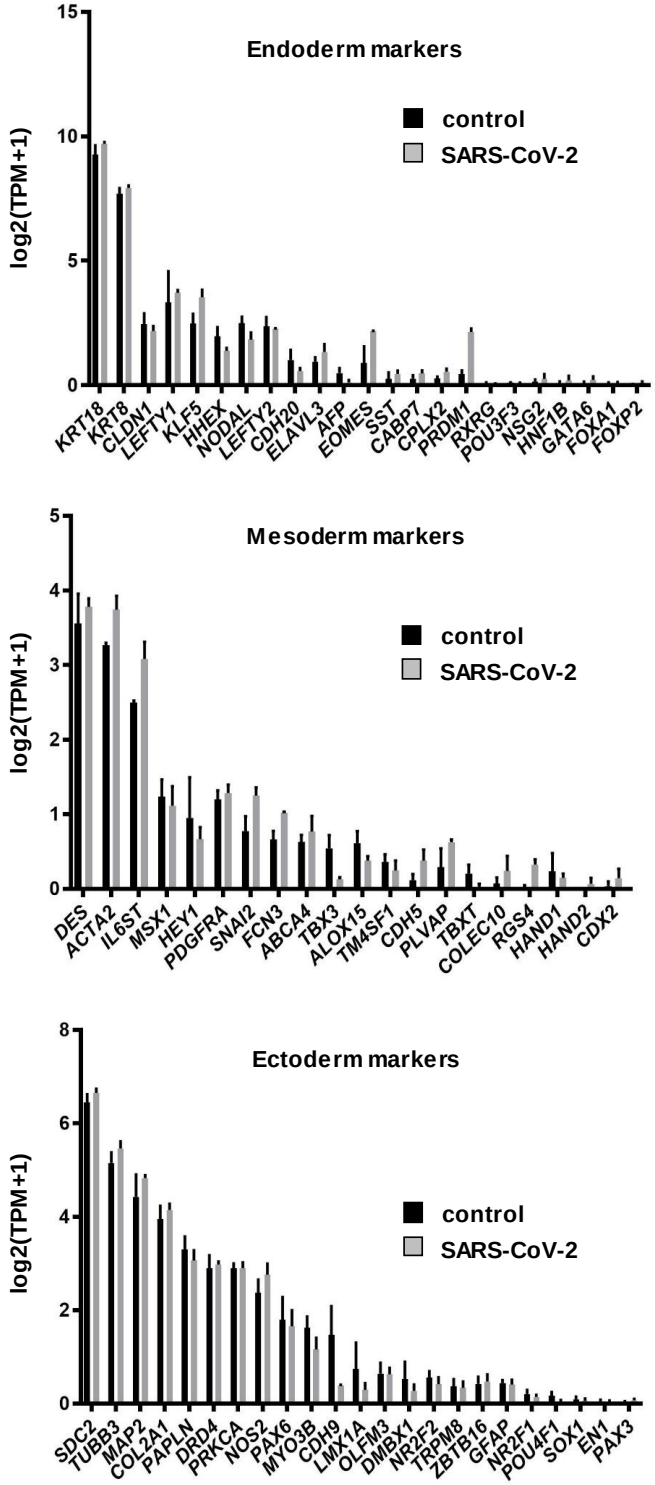

Figure S7 Gene expression profiles of endoderm, mesoderm, and ectoderm markers in infected ACE2-iPS cells, Related to Figure 4

RNA-seq analysis of uninfected and infected ACE2-iPS cells. Bar plots of ectoderm, mesoderm, and endoderm markers in uninfected ACE2-iPS cells (control) and infected ACE2-iPS cells (SARS-CoV-2) are shown.

Supplemental tables

Table S1 Drugs used in the infection experiments, Related to Figure 6

Drug	Catalogue	Company
Camostat mesylate	SML0057	Sigma-Aldrich
Chloroquine diphosphate	No.4109	Tocris
EIDD-2801	HY-135853	MedChemExpress
Favipiravir	S7975	Selleck Chemicals
Ivermectin	I8618	LKT Labs
Nafamostat mesylate	N0289-10MG	Sigma-Aldrich
Recombinant human IFN-β	300-02BC	PeproTech
Remdesivir	A17170	Clinisciences

Table S2 Primers used in this study, Related to Figures 3, 6, S1, S2, and S4

Gene name	Fwd primer	Rev primer
ACE2	ACAGTCCACACTTGCCCAAAT	TGAGAGCACTGAAGACCCATT
CD147	GAAGTCGTCAGAACACATCAACG	TTCCGGCGCTTCTCGTAGA
CER1	ACAGTGCCCTTCAGCCAGACT	ACAACTACTTTTTCACAGCCTTCGT
FOXA2	GCGACCCCAAGACCTACAG	GGTTCTGCCGGTAGAAGGG
GAPDH	GGAGCGAGATCCCTCCAAAAT	GGCTGTTGTCATACTTCTCATGG
IFNα	GCCTCGCCCTTTGCTTTACT	CTGTGGGTCTCAGGGAGATCA
IFNβ	ATGACCAACAAGTGTCTCCTCC	GGAATCCAAGCAAGTTGTAGCTC
ISG15	CGCAGATCACCCAGAAGATCG	TTCGTCGCATTTGTCCACCA
NANOG	AGAAGGCCTCAGCACCTAC	GGCCTGATTGTTCCAGGATT
NRP1	GGCGCTTTTCGCAACGATAAA	TCGCATTTTTCACTTGGGTGAT
OCT3/4	CTTGAATCCCGAATGGAAAGGG	GTGTATATCCCAGGGTGATCCTC
SARS-CoV-N	CCAGGTAACAAACCAACCAACTTTCG	GGTTACTGCCAGTTGAATCTGAGG
SOX17	GTGGACCGCACGGAATTTG	GAGGCCCATCTCAGGCTTG
SOX2	GGCAGCTACAGCATGATGATGCAGGAGC	CTGGTCATGGAGTTGTACTGCAGG
TMPRSS2	GTCCCCACTGTCTACGAGGT	CAGACGACGGGGTTGGAAG

Table S3 Antibodies used in this study, Related to Figures 3, S2, and S5

Antigen	Catalogue	Host	Company
Donkey anti-Mouse IgG (H+L) Highly Cross-Adsorbed Secondary Antibody, Alexa Fluor Plus 594	A32744	Donkey	Thermo Fisher Scientific
Goat anti-Rabbit IgG (H+L) Highly Cross-Adsorbed Secondary Antibody, Alexa Fluor Plus 488	A32731	Goat	Thermo Fisher Scientific
OCT3/4	sc-5279	Mouse	Santa Cruz Biotechnology
SARS-CoV-2 NP	A2061-50	Rabbit	BIO Vision
SOX2	sc-365823	Mouse	Santa Cruz Biotechnology
Tra1-81	MAB4381	Mouse	Sigma-Aldrich

Transparent methods

Materials availability

All unique/stable reagents generated in this study are available from the corresponding authors with a completed Materials Transfer Agreement.

Human ES/iPS cells

The human ES/iPS cell lines 1383D6 (Nakagawa et al., 2014) (provided by Dr. Masato Nakawaga, Kyoto University), 201B7 (Takahashi et al., 2007), Tic (JCRB1331, JCRB Cell Bank), H1 (WA01), H9 (WA09) (WiCell Research Institute), KhES1, KhES2, and KhES3 (Kyoto University) were maintained on 0.5 μg/cm^2 recombinant human laminin 511 E8 fragments (iMatrix-511, Nippi) with StemFit AK02N medium (Ajinomoto) containing 10 μM Y-27632 (from day 0 to day 1, FUJIFILM Wako Pure Chemical). To passage human ES/iPS cells, near-confluent human ES/iPS cell colonies were treated with TrypLE Select Enzyme (Thermo Fisher Scientific) for 5 min at 37°C. After the centrifugation, the cells were seeded at an appropriate cell density (1.3×10^4 cells/9 cm^2) onto iMatrix-511 and subcultured every 6 days. Human ES cells were used following the Guidelines for Derivation and Utilization of Human Embryonic Stem Cells of the Ministry of Education, Culture, Sports, Science and Technology of Japan, and the study was approved by an independent ethics committee. Except for **figure 6**, the human iPS cell line 1383D6 was used for all experiments.

SARS-CoV-2 preparation

The SARS-CoV-2 strains used in this study (SARS-CoV-2/Hu/DP/Kng/19-027) were provided by the Kanagawa Prefectural Institute of Public Health. SARS-CoV-2 was isolated from a COVID-19 patient (GenBank: LC528233.1). The isolation and analysis of the virus will be described elsewhere (manuscript in preparation). The virus was plaque-purified and propagated in Vero cells and stored at -80°C. All experiments including virus infections were done in a biosafety level 3 facility at Kyoto University strictly following regulations.

Adenovirus vectors

Ad vectors were constructed using Adeno-X^{TM} Adenoviral System 3 (Takara Bio). The ACE2 and TMPRSS2 genes were amplified by PCR using cDNA generated from Pulmonary Alveolar Epithelial Cell Total RNA (ScienCell Research Laboratories) as a template. The ACE2 and TMPRSS2 genes were inserted into Adeno-X^{TM}

Adenoviral System 3, resulting in pAdX-ACE2 and pAdX-TMPRSS2, respectively. The ACE2- and TMPRSS2-expressing Ad vectors (Ad-ACE2 and Ad-TMPRSS2, respectively) were propagated in HEK293 cells (JCRB9068, JCRB Cell Bank). LacZ-expressing Ad vectors were purchased from Vector Biolabs. The vector particle (VP) titer was determined by using a spectrophotometric method (Maizel Jr et al., 1968).

Viral titration of SARS-CoV-2

Viral titers were measured by median tissue culture infectious dose (TCID50) assays at a biosafety level 3 laboratory (Kyoto University). TMPRSS2/Vero cells (JCRB1818, JCRB Cell Bank) (Matsuyama et al., 2020) were cultured with Minimum Essential Media (MEM, Sigma-Aldrich) supplemented with 5% fetal bovine serum (FBS), and 1% penicillin/streptomycin and seeded into 96-well cell culture plates (Thermo Fisher Scientific). The samples were serially diluted 10-fold from 10^{-1} to 10^{-8} in the cell culture medium. Dilutions were placed onto the TMPRSS2/Vero cells in triplicate and incubated at 37°C for 96 hr. Cytopathic effects were evaluated under a microscope. TCID50/mL was calculated using the Reed-Muench method.

Quantification of viral RNA copy number

The cell culture supernatant was mixed with an equal volume of 2×RNA lysis buffer (distilled water containing 0.4 U/uL SUPERase I^{TM} RNase Inhibitor (Thermo Fisher Scientific), 2% Triton X-100, 50 mM KCl, 100 mM Tris-HCl (pH 7.4), and 40% glycerol) and incubated at room temperature for 10 min. The mixture was diluted 10 times with distilled water. Viral RNA was quantified using a One Step TB Green PrimeScript PLUS RT-PCR Kit (Perfect Real Time) (Takara Bio) on a StepOnePlus real-time PCR system (Thermo Fisher Scientific). The primers used in this experiment are as follows: (forward) AGCCTCTTCTCGTTCCTCATCAC and (reverse) CCGCCATTGCCAGCCATTC. Standard curves were prepared using SARS-CoV-2 RNA (10^5 copies/μL) purchased from Nihon Gene Research Laboratories.

Ultrathin section transmission electron microscopy (TEM)

Uninfected and infected ACE2-iPS cells were fixed with 2.5% glutaraldehyde in 0.1M cacodylate buffer and subsequently post-fixed with 1% osmium tetroxide in the same buffer for 1 hr at 4°C. After fixation, they were dehydrated in a series of ethanol gradient and embedded in epoxy resin. Ultrathin sections were cut, stained with uranyl acetate and lead citrate, and examined using an electron microscope (HITACHI HT-7700) at 80 kV.

RNA-seq

Total RNA was prepared using an RNeasy Mini Kit (Qiagen). RNA integrity was assessed with a 2100 Bioanalyzer (Agilent Technologies). The library preparation was performed using a TruSeq stranded mRNA sample prep kit (Illumina) according to the manufacturer's instructions. Sequencing was performed on an Illumina NextSeq500. The fastq files were generated using bcl2fastq-2.20. Adapter sequences and low-quality bases were trimmed from the raw reads by Cutadapt ver 1.14 (Martin, 2011). The trimmed reads were mapped to human reference genome sequences (hg38) using STAR ver 2.5.3a (Dobin et al., 2013) with the GENCODE (release 36, GRCh38.p13) (Frankish et al., 2019) gtf file. The raw counts for protein-coding genes were calculated using htseq-count ver. 0.12.4 (Anders et al., 2015) with the GENCODE gtf file. Gene expression levels were determined as transcripts per million (TPM) with DEseq2 (Love et al., 2014). Raw data concerning this study were submitted under Gene Expression Omnibus (GEO) accession number GSE166990.

SARS-CoV-2 infection and drug treatment

ACE2-iPS cells and Vero cells (JCRB0111, JCRB Cell Bank) cultured in a 96-well plate (2.0×10^4 cells/well) were infected with 2.0×10^3 TCID50/well of SARS-CoV-2 for 2 hr and then cultured with medium containing drugs. In the infection and drug treatment experiments, the medium containing drugs was replaced with fresh medium every day. At day 2 (Vero cells) or day 4 (ACE2-iPS cells) after the infection, the viral RNA copy number in the cell culture supernatant was measured by qPCR. Drugs used in the infection experiments are summarized in **Table S1**.

Quantitative PCR

Total RNA was isolated from human iPS cells using ISOGENE (NIPPON GENE). cDNA was synthesized using 500 ng of total RNA with a Superscript VILO cDNA Synthesis Kit (Thermo Fisher Scientific). Real-time RT-PCR was performed with SYBR Green PCR Master Mix (Thermo Fisher Scientific) using a StepOnePlus real-time PCR system (Thermo Fisher Scientific). The relative quantitation of target mRNA levels was performed by using the $2^{-\Delta\Delta CT}$ method. The values were normalized by those of the housekeeping gene, *glyceraldehyde 3-phosphate dehydrogenase* (*GAPDH*). The PCR primer sequences are shown in **Table S2**.

Immunofluorescence staining

For the immunofluorescence staining of human iPS cells, the cells were fixed with 4% paraformaldehyde in PBS at 4°C. After blocking the cells with PBS containing 2% bovine serum albumin and 0.2% Triton X-100 at room temperature for 45 min, the cells were incubated with a primary antibody at 4°C overnight and then with a secondary antibody at room temperature for 1 hr. All antibodies used in this report are described in **Table S3**.

Statistical analyses

Statistical significance was evaluated by unpaired two-tailed Student's *t*-test or one-way analysis of variance (ANOVA) followed by Tukey's post hoc tests. Statistical analyses were performed using GraphPad Prism8 and 9. Data are representative of three independent experiments. Details are described in the figure legends.

Supplemental references

Anders, S., Pyl, P.T., and Huber, W. (2015). HTSeq—a Python framework to work with high-throughput sequencing data. Bioinformatics *31*, 166-169.

Dobin, A., Davis, C.A., Schlesinger, F., Drenkow, J., Zaleski, C., Jha, S., Batut, P., Chaisson, M., and Gingeras, T.R. (2013). STAR: ultrafast universal RNA-seq aligner. Bioinformatics *29*, 15-21.

Frankish, A., Diekhans, M., Ferreira, A.-M., Johnson, R., Jungreis, I., Loveland, J., Mudge, J.M., Sisu, C., Wright, J., and Armstrong, J. (2019). GENCODE reference annotation for the human and mouse genomes. Nucleic acids research *47*, D766-D773.

Love, M.I., Huber, W., and Anders, S. (2014). Moderated estimation of fold change and dispersion for RNA-seq data with DESeq2. Genome biology *15*, 1-21.

Maizel Jr, J.V., White, D.O., and Scharff, M.D. (1968). The polypeptides of adenovirus: I. Evidence for multiple protein components in the virion and a comparison of types 2, 7A, and 12. Virology *36*, 115-125.

Martin, M. (2011). Cutadapt removes adapter sequences from high-throughput sequencing reads. EMBnet journal *17*, 10-12.

Matsuyama, S., Nao, N., Shirato, K., Kawase, M., Saito, S., Takayama, I., Nagata, N., Sekizuka, T., Katoh, H., and Kato, F. (2020). Enhanced isolation of SARS-CoV-2 by TMPRSS2-expressing cells. Proceedings of the National Academy of Sciences *117*, 7001-7003.

Nakagawa, M., Taniguchi, Y., Senda, S., Takizawa, N., Ichisaka, T., Asano, K., Morizane, A., Doi, D., Takahashi, J., and Nishizawa, M. (2014). A novel efficient feeder-free culture system for the derivation of human induced pluripotent stem cells. Scientific reports *4*, 1-7.

Takahashi, K., Tanabe, K., Ohnuki, M., Narita, M., Ichisaka, T., Tomoda, K., and Yamanaka, S. (2007). Induction of pluripotent stem cells from adult human fibroblasts by defined factors. cell *131*, 861-872.